Atmospheric
Measurement
Techniques

Correcting 3D cloud effects in X_{CO_2} retrievals from the Orbiting Carbon Observatory-2 (OCO-2)

Steffen Mauceri[1], Steven Massie[2], and Sebastian Schmidt[2]

[1]Jet Propulsion Laboratory, California Institute of Technology, Pasadena, CA 91109, USA
[2]Laboratory for Atmospheric and Space Physics, University of Colorado, Boulder, CO 80303, USA

Correspondence: Steffen Mauceri (steffen.mauceri@jpl.nasa.gov)

Abstract. The Orbiting Carbon Observatory-2 (OCO-2) makes space-based radiance measurements in the oxygen A band and the weak and strong carbon dioxide (CO_2) bands. Using a physics-based retrieval algorithm these measurements are inverted to column-averaged atmospheric CO_2 dry-air mole fractions (X_{CO_2}). However, the retrieved X_{CO_2} values are biased due to calibration issues and mismatches between the physics-based retrieval radiances and observed radiances. Using multiple linear regression, the biases are empirically mitigated. However, a recent analysis revealed remaining biases in the proximity of clouds caused by 3D cloud radiative effects (Massie et al., 2021) in the processing version B10. Using an interpretable non-linear machine learning approach, we develop a bias correction model to address these 3D cloud biases. The model is able to reduce unphysical variability over land and sea by 20 % and 40 %, respectively. Additionally, the 3D cloud bias-corrected X_{CO_2} values show agreement with independent ground-based observations from the Total Carbon Column Observation Network (TCCON). Overall, we find that the published OCO-2 data record underestimates X_{CO_2} over land by −0.3 ppm in the tropics and northward of 45° N. The approach can be expanded to a more general bias correction and is generalizable to other greenhouse gas experiments, such as GeoCarb, GOSAT-3, and CO2M.

1 Introduction

The Orbiting Carbon Observatory-2 (OCO-2; Eldering et al., 2017; Crisp et al., 2004) makes space-based top-of-atmosphere radiance measurements in three spectral bands: oxygen A band at 0.76 µm, the weak CO_2 band at 1.61 µm, and the strong CO_2 band at 2.06 µm. Using an optimal estimation retrieval (Rodgers, 2000) called ACOS (O'Dell et al., 2018), these measurements are converted to column-averaged atmospheric CO_2 dry-air mole fractions (X_{CO_2}). ACOS employs a physics-based forward model that takes into consideration viewing and solar geometry and various atmospheric and surface parameters. Since OCO-2 generates on the order of 100 000 soundings per day, ACOS makes multiple approximations to speed up the retrieval algorithm. Most importantly, the retrieval makes the independent pixel approximation, where the radiance in a given sounding only depends on the properties (e.g., surface pressure, surface reflectance, aerosols, trace gas concentration) within the field of view of this sounding. This approximation exploits the fact that for most clear-sky observations there is no significant horizontal exchange of photons.

Nearby clouds, however, can scatter a significant number of photons into the field of view of OCO-2, which enhances the observed radiance. This horizontal exchange of photons due to clouds, or the 3D cloud effect, is not accounted for in the ACOS retrieval. Nevertheless, the forward model attempts to match the enhanced radiances, which leads to errors in the converged state vector and, most importantly, negative biases in retrieved X_{CO_2} (Massie et al., 2021, 2017; Merrelli et al., 2015; Emde et al., 2022; Kylling et al., 2022; Yu et al., 2022). Merrelli et al. (2015) applied the spherical-

harmonics discrete-ordinate method (SHDOM) 3D radiative transfer code (Evans, 1998) to perturb OCO-2 type spectra and calculated OCO-2 retrievals without and with the 3D radiance perturbations. Retrieved X_{CO_2} values were *lower* than clear-sky retrievals by 0.3, 3, and 5–6 ppm for surfaces characterized by bare soil, vegetation, and snow-covered footprints, respectively. From an empirical perspective, Fig. 6 of Massie et al. (2021) demonstrates that retrieved X_{CO_2} over sea generally decreases when the distance between observations and clouds becomes less than 5 km.

Nearby clouds can also cause radiance dimming due to cloud shadows. Cloud brightening occurs on both sides of clouds since 40 % of OCO-2 observations are within 4 km of clouds (Massie et al., 2021), and cloud brightening extends over a 5 to 10 km horizontal scale. A cloud shadow occurs only on one side of a cloud, with the shadow covering a limited angular portion of the side. Since the majority of OCO-2 observations are next to low-level clouds (think of an observation embedded in low-level Amazon cloud streets), the cloud shadows project only about 1 km or so from the low-level clouds. Using a year's data volume, Massie et al. (2022) discuss detailed calculations, based on an analysis of OCO-2 O_2 A-band continuum radiances, that yield an estimate of cloud shadowing frequency to be on the order of 4 %, compared to 96 % for the observations influenced by cloud brightening.

To mitigate biases in retrieved "raw" X_{CO_2}, a linear bias correction and threshold-based filtering are applied to the data, yielding "bias-corrected" X_{CO_2}. Bias correction and filtering are based on co-retrieved elements from the state vector that are used to bring retrieved X_{CO_2} into agreement with multiple truth sources (Kiel et al., 2019). These truth sources include a "small-area analysis", which assumes that X_{CO_2} is constant over small distances (< 100 km) within the same orbit; comparisons to ground-based observations from the Total Carbon Column Observation Network (TCCON) (Wunch et al., 2010); and comparisons to a multi model-mean of six models that assimilate in situ data. Nevertheless, there are remaining underestimates in retrieved X_{CO_2} that have been linked to 3D cloud effects in the proximity of clouds with an average of −0.4 and −2.2 ppm for high-quality and low-quality data (Massie et al., 2021). To address these biases Massie et al. (2021) developed a linear bias correction and filtering approach using a set of features indicative of 3D cloud effects calculated from Moderate Resolution Imaging Spectroradiometer (MODIS) and OCO-2 files. However, biases in X_{CO_2} caused by nearby clouds are highly non-linear. Consequently, the present study has two goals. The first goal is to explore if a non-linear bias correction can reduce 3D cloud biases more than a linear approach. While the developed cloud features (normalized standard deviation of the radiance field – H3D, differences in continuum radiances of an observation to adjacent observations – HC, ratio of continuum radiance spatial standard deviation and noise level – CSNoiseRatio, cloud distance; discussed below) more di-

rectly capture 3D cloud effects, co-retrieved variables from the state vector might be more indicative of the resulting X_{CO_2} biases. Thus, the second goal is to investigate if additional variables, co-retrieved with X_{CO_2}, can be used to further reduce 3D cloud biases.

2   Data

We make use of OCO-2 (B10) (https://disc.gsfc.nasa.gov/datasets/OCO2_L2_Lite_FP_10r/summary, last access: 13 March 2023) data from September 2014 to July 2019. These files contain bias-corrected X_{CO_2} for soundings over sea in glint mode (in which sunlight is directly reflected by the Earth's surface towards OCO-2) and soundings over land with a nadir viewing geometry. We correct for remaining 3D cloud biases by utilizing a variety of parameters describing the retrieved atmospheric state vector, viewing and solar geometry, results from OCO-2 cloud screening pre-processors, location and time, and a quality flag (QF) for each sounding. The QF is determined by a series of hand-tuned thresholds for various variables derived from state vector elements that are indicative of retrieval biases in X_{CO_2}. High-quality data have a QF = 0, and low-quality data have QF = 1. Similarly, the operational bias correction is performed with hand-tuned linear fits to various state vector elements (Kiel et al., 2019).

In addition, we utilize ground-based observations by TCCON from all 27 stations that are in close proximity in time (24 h) and space (2.5° in latitude, 5° in longitude) to OCO-2 observations (https://tccondata.org/, last access: 13 March 2023; Total Carbon Column Observing Network (TCCON) Team, 2017). The ground-based observations are used for validation only. However, they can only provide comparisons for a limited number of locations, with relatively few ground-based sites in the tropics and island locations.

Finally, we make use of four variables indicative of 3D cloud effects (Massie et al., 2021): H3D, HC, CSNoiseRatio, and cloud distance. H3D (Liang et al., 2009; Massie et al., 2017) describes the normalized standard deviation of the MODIS radiance field and is calculated based on offline MODIS radiance data files (Cronk, 2018). The radiance standard deviation is calculated in a circle with a radius of 10 km surrounding each OCO-2 data point. HC is calculated from differences in O_2 A-band continuum radiances of an observation point and adjacent points in three rows (frames) of footprints. A frame has eight adjacent OCO-2 footprints, with each footprint on the order of 2 km in size. CSNoiseRatio is the ratio of the O_2 A-band continuum radiance spatial standard deviation and noise level, calculated within a footprint (which has 20 "ColorSlice" sub-pixel elements). These three variables are indicative of 3D cloud effects since radiance gradients are present when clouds are next to observation footprints (radiance enhancements become larger as cloud distance decreases). Cloud distance (Massie et al., 2021) is the distance of the nearest cloud to

each observation point, as determined from offline radiance data files (Cronk, 2018), which contain 500 m MODIS radiances, geolocation, and cloud mask data. Calculated 3D cloud features can be found for OCO-2 from September 2014 to July 2019 at https://doi.org/10.5281/zenodo.4008764 (Massie et al., 2020).

3   Methods

3.1   Small areas and TCCON as truth metric

As a pre-processing step we match the 3D cloud variables, OCO-2 soundings, and TCCON by time and location. Afterwards, we remove soundings where no 3D cloud variables are available. To develop the bias correction model, we use the small-area analysis, which is based on the assumption that CO_2 is a well-mixed gas and assumed to be constant over spatial scales of less than ~ 100 km (though there can be exceptions for strong CO_2 emitters such as megacities). To exploit this constraint on X_{CO_2} we split OCO-2 soundings from the same orbit into small areas with a maximum size of 100 km. Each small area is generated by collecting soundings (sorted by observation time) until the distance between the first and last sounding exceeds the 100 km threshold. Afterwards, the collection process of the next small area is started. For each small area we identify soundings that are assumed to be free of 3D cloud biases (nearest cloud is at least 10 km away). From those soundings we define the median retrieved X_{CO_2} as the true X_{CO_2} of a given small area, and any differences to this median are treated as biases. Small areas that contain fewer than 10 soundings free of 3D cloud biases are removed from the data set. Since this process biases the remaining small areas towards longer cloud distances, we resample the remaining soundings so that the distribution of nearest-cloud distances is similar to the original data set, with about 40 % of the sounding having a nearest-cloud distance of less than 4 km. Note that this processing will interpret real X_{CO_2} enhancements, for example from power plants, as positive biases. However, we postulate that these cases are rare and that a model that is robust to outliers can still learn a useful bias correction from these data. Next, we remove outliers with large X_{CO_2} errors from the data set by applying a series of thresholds to the variables from the state vector. The variables and their thresholds are given in Table 1. Note that these filters remove only a small fraction of soundings (4 %). Finally, we remove small areas with fewer than 20 soundings. This results in approximately 5×10^6 soundings over land and 20×10^6 soundings over the ocean, with a small subset of the soundings having coincident TCCON measurements. TCCON can only provide comparison for a limited set of regions, with most stations in the Northern Hemisphere and over land. This challenges the development of a bias correction approach based on X_{CO_2}–TCCON differences that would be representative of areas far away from existing sta-

tions, such as Africa, South America, and most of the ocean. Therefore, we use TCCON only as an independent truth metric for validation and not to develop the model itself.

The distribution of nearest-cloud distance, biases from the small-area analysis, and comparison to TCCON for land nadir and sea glint observations with QF = 0 and QF = 1 are shown in Fig. 1. The plots show that the majority of OCO-2 soundings are taken within close proximity of clouds and that many of those soundings are filtered out in the current OCO-2 product (QF = 1). This is especially problematic for areas such as the tropics that are dominated by clouds and, as a result, have few valid soundings. The small-area and TCCON biases for QF = 0 data are roughly normally distributed, with a mean and standard deviation of 0.0 ± 0.5 ppm for small-area biases and 0.2 ± 0.8 ppm compared to TCCON for soundings over sea. For soundings over land the small-area bias and bias compared to TCCON are similar, with a mean and standard deviation of $0.1 \pm \sim 1$ ppm. For QF = 1 the distribution of biases has a larger standard deviation for small-area biases (land: 2.7 ppm; sea: 1.8 ppm) and, compared to TCCON (land: 3.7 ppm; sea: 1.9 ppm), is skewed and contains negative biases that far exceed positive biases, as analyzed with the small areas (land: -0.6 ppm; sea: -1.2 ppm) and compared to TCCON (land: -1.2 ppm; sea: -1.2 ppm). This long-tail distribution of negative biases is indicative of 3D cloud effects (Massie et al., 2021) and should be mitigated with a successful 3D cloud bias correction.

3.2   Train, validation, test split

To fit, or *train*, the bias correction model we used soundings from September 2014 to the end of July 2017, totaling roughly 12×10^6 and 3×10^6 soundings over sea and land, respectively. To find the best model parameters and evaluate what features minimize biases the furthest we use a separate validation set containing soundings from the beginning of August 2017 to the end of July 2018. Finally, to test how the trained model performs on new data we use a separate testing set of soundings from the beginning of August 2018 to the end of July 2019. The validation and testing set have 3×10^6 and 2×10^6 soundings over the sea with QF = 0 and QF = 1, respectively, and 5×10^5 soundings each over land with QF = 0 and QF = 1.

3.3   Bias correction model

We train two types of models for the bias correction, nonlinear models (random forest) and linear models (ridge regression), to provide a baseline comparison. A random forest is an ensemble of classifying decision trees and outputs the mean of those trees (Breiman, 2001). Random forests are easy to interpret and robust to outliers. Each tree is trained in a supervised manner with a random subset (50 %) of the available training data, also referred to as bootstrapping. Using the training data, each tree iteratively splits the data us-

Table 1. Variables and their thresholds used to remove outliers.

Variable	Description	Land	Sea
co2_ratio	Ratio of retrieved X_{CO_2} in WCO_2 and SCO_2 bands	$x < 1$ or $x > 1.04$	$x < 1$ or $x > 1.03$
co2_grad_del	Change between the retrieved CO_2 profile and the a priori profile	$x < -100$ or $x > 100$	$x < -50$ or $x > 100$
deltaT	Retrieved offset to a priori temperature profile		$x < 0$
dpfrac	Retrieved X_{CO_2} multiplied by difference in retrieved and a priori surface pressure (Kiel et al., 2019)	$x > 7$	
rms_rel_sco2	Root mean square error in the L2 fit residuals for the SCO_2 band, relative to the continuum signal		$x > 0.5$
snr_sco2	Signal-to-noise ratio in SCO_2 band		$x < 200$
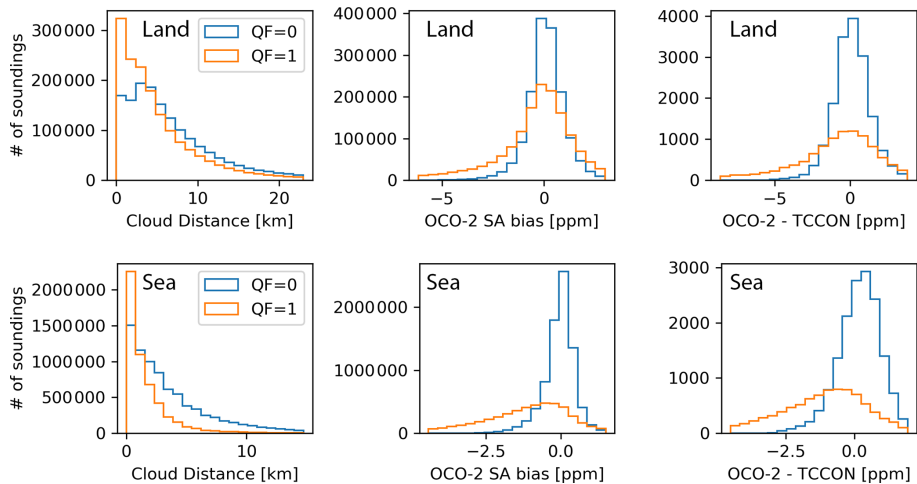
Figure 1. Histogram of data used in this study for nearest-cloud distance (left), small-area (SA) biases (middle), and biases compared to TCCON (right) for soundings over land (top) and sea (bottom). Higher-quality data (QF = 0) are shown in blue, and lower-quality data (QF = 1) are shown in orange.

ing the feature that can minimize the mean square error in the predictions the furthest until it reaches a maximum user-provided number of splits, or *depth*. For our land model we used a depth of 8 and for our ocean model a depth of 15. The larger model size for the ocean is mostly due to there being more training data available over the ocean than over land, which allows a larger model that still generalizes to be fit to new data. Each random forest was composed of 100 individual trees. These parameters were chosen to maximize model performance on the validation set. The model inputs are a set of selected features from the OCO-2-retrieved state vector (e.g., *co2_grad_del*), and the model output is the remaining X_{CO_2} bias derived from the small-area analysis.

Since the operational OCO-2 bias correction uses a linear approach, we also perform a baseline comparison to a linear model. We choose multivariate linear regression with a small Tikhonov regularization term (the regularization helps if some of the inputs are correlated, which is the case for most real-world applications), also referred to as ridge regression

(Hoerl and Kennard, 1970b, a). Thus, using the training set we seek to find the weights, w, that minimize the following equation:

$$\|y - Xw\|_2^2 + \alpha\|w\|_2^2,\tag{1}$$

where y is the standardized (mean removed and divided by standard deviation) X_{CO_2} bias, X represents the standardized features, $\|\cdot\|_2$ is the Euclidean norm, and α controls the strength of the Tikhonov regularization. For our application we found that $\alpha = 10^{-5}$ maximizes performance for the validation set.

3.4 Feature selection

First, we identified retrieved state variables that show a strong dependence (change in mean or variability) on nearest-cloud distance, indicating that they might be good candidates to correct for 3D cloud effects. Two examples are shown in Fig. 2. In addition to the list of identified features we added solar and viewing geometries and surface

albedo. Those variables have a direct physical impact on 3D cloud effects; 3D cloud effects are amplified at large solar zenith angles and for brighter surfaces (Okata et al., 2017). Finally, we removed highly correlated variables. This results in a set of 23 features for soundings over land and 24 features for soundings over sea that may be used to correct for 3D cloud biases in retrieved X_{CO_2} (more information about each variable can be found on pp. 29 to 40 in Jet Propulsion Laboratory, 2018). Next, we used *recursive feature elimination* to identify what subset of features can reduce biases the furthest. Reducing the number of features makes the model more robust to new data, avoids *overfitting,* and aids interpretability.

For the recursive feature elimination, we removed one feature at a time and trained a small random forest model with 32 trees each on a random selection of 5×10^5 soundings with $QF = 0$ and $QF = 1$ from the training set. Afterwards we calculated the model performance on the full validation set. As the performance metrics we used the correlation coefficient (R^2) between modeled bias and existing bias as indicated by the small-area calculations. The feature that has been removed from the highest-performing model is then permanently removed, and the process is repeated until only one feature is left. The iterative process was performed separately for land and sea soundings. The order of the feature elimination and resulting R^2 is shown in Fig. 3. The least important variables are shown at the top and were removed first. A low importance can either result from a variable varying independently of biases in X_{CO_2}, or the variable could be correlated with another variable (e.g., *dp* and *dp_abp*) or set of variables that provide similar information, making one of them obsolete. The most important variables are shown on the bottom.

For our bias correction model we decided to use the five most important variables for land and four most important variables for sea soundings, as identified by the feature elimination. These variables explain most of the variance and partially overlap for land and sea. For land the most important variables are dp_abp (retrieved surface pressure from pre-processor retrieval minus surface pressure from the GEOS-5 FP-IT model), *h2o_ratio* (ratio of retrieved H_2O column from the WCO$_2$ band to that from the SCO$_2$ band), co2_grad_del (a measure of the difference in the retrieved and prior CO_2 vertical gradient), dp (retrieved surface pressure from the L2 full-physics retrieval minus the O$_2$ A-band prior surface pressure), and *aod_water* (retrieved extinction optical depth of cloud water at 755 nm). For sea the most important variables are dp, co2_grad_del, *aod_ice* (retrieved extinction optical depth of cloud ice at 755 nm), and *albedo_wco2* (retrieved Lambertian albedo in the WCO$_2$ band). Note that the final set of features does not include any of the 3D cloud metrics used in the bias correction discussed in Massie et al. (2021). Additionally, solar and viewing geometry was removed in the iterative process. However, the process includes the surface albedo in the weak CO$_2$

band, dp, and dp_abp, which have a direct physical connection to 3D cloud effects. As discussed below in relation to Fig. 2b, dp_abp and nearest-cloud distance are empirically correlated. Additionally, increased values in aod_water and deviations from unity for h2o_ratio are indicative of cloud contamination (Jet Propulsion Laboratory, 2018). This indicates that elements of the operational retrieval state vector (co2_grad_del, dp, dp_abp, h2o_ratio, aod_water, aod_ice, albedo_wco2) are more directly correlated with remaining biases in X_{CO_2} (due to 3D cloud and other effects) than features that directly measure 3D cloud effects which perturb the radiation field (H3D, HC, CSNoiseRatio).

From an operational standpoint, using elements from the current retrieval state vector to correct 3D cloud biases simplifies the bias correction in future operational products. It is also more generally applicable to other missions that might not have available coincident cloud field measurements that can be applied to derive nearest-cloud distances, such as OCO-3 (Eldering et al., 2019). On the other hand, it reduces the interpretability of the developed model and does not allow 3D cloud biases to be directly linked to 3D cloud metrics. The OCO-2 and 3D cloud variables and their meaning are summarized in Table 2.

Note that it is not possible to clearly separate biases due to 3D cloud effects and other mismatches between the forward model of the retrieval algorithm and the observed radiances. For example, differences in modeled and real aerosol optical properties (Chen et al., 2022) or uncertainties in absorption profiles of various trace gases (Payne et al., 2020) are likely important. Additionally, uncertainties in the instrument calibration can cause systematic biases as well. Thus, some of the features might also correct for non-3D cloud effects. However, we tried to mitigate the effect of non-3D cloud biases by only adding features to the feature selection process that show some dependence on nearest-cloud distance (see Fig. 2) or have a direct physical relationship to 3D cloud biases. Additionally, our bias correction is applied to data that have already been corrected with the operational OCO-2 bias correction (our processing utilizes bias-corrected X_{CO_2}). Thus, biases independent of 3D cloud effects should be minimized.

4 Results

4.1 Reduction in X_{CO_2} biases

After the random forest was trained using the training set (September 2014–July 2017) we evaluated the model performance on the testing set (August 2018–July 2019). Figure 4 compares remaining X_{CO_2} biases in OCO-2 (as determined by the small-area analysis) with biases after our correction is applied (OCO-2 corr.) for $QF = 0$ and $QF = 1$ soundings. For land soundings X_{CO_2} biases are reduced from a root mean square error (RMSE) of 2.0 to 1.6 ppm (see Fig. 4c). For sea

Table 2. Summary of OCO-2 state vector variables and 3D cloud variables.

Variables	Description
dp_abp	Retrieved surface pressure from pre-processor retrieval, minus surface pressure from forecast model
dp	Retrieved surface pressure from full-physics retrieval, minus surface pressure from O_2 A-band prior
h2o_ratio	Ratio of retrieved H_2O column from WCO_2 band to SCO_2 band
co2_grad_del	Change between retrieved CO_2 profile and a priori profile
aod_water	Retrieved extinction optical depth of cloud water
aod_ice	Retrieved extinction optical depth of cloud ice
albedo_wco2	Retrieved surface albedo in WCO_2 band
H3D	Normalized standard deviation of the radiance field
HC	Differences in continuum radiances of an observation to adjacent observations
CSNoiseRatio	Ratio of continuum radiance spatial standard deviation and noise level
Cloud distance	Distance to the nearest cloud
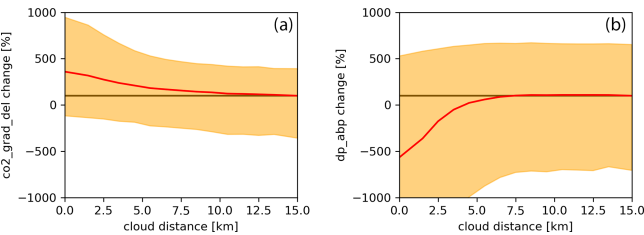
Figure 2. Change in variability and mean in percent of potential features with respect to nearest-cloud distance. Change in mean is shown in red; change in the 5th and 95th percentile is shown in yellow; no change (baseline) is shown with a straight brown line. Change is calculated with respect to feature mean for observations with a nearest-cloud distance of 14 to 15 km. Panel **(a)** shows co2_grad_del, and panel **(b)** shows dp_abp. Please refer to the text for a description of the two features.

soundings the bias correction has a significantly bigger impact and reduces biases from 1.4 to 0.9 ppm (see Fig. 4d). Over the sea the bias correction mostly corrects negative biases less than -0.8 ppm (see Fig. 4b).

Table 3 shows the RMSE by quality flag. For QF = 0 and QF = 1 the biases in X_{CO_2} corrected with our model are less than the testing set operational OCO-2 biases. However, for QF = 0 improvements by our correction (OCO-2 corr.) compared to OCO-2 are small ($< 10\%$). The QF = 0 data have significantly fewer soundings with clouds in close proximity (see Fig. 1), which explains in part the smaller difference. Additionally, the quality flags are determined so that the operational linear bias correction of OCO-2 works well; i.e., X_{CO_2} biases have a mostly linear relationship to elements of the state vector where QF = 0. For QF = 1 the difference is more significant, reducing the RMSE from 2.6 to 2.1 ppm over land and from 2.3 to 1.3 ppm over sea.

To more directly link the bias correction to 3D cloud effects we show biases with respect to nearest-cloud distance in Fig. 5. X_{CO_2} from OCO-2 shows a clear negative mean bias and increased variance for a nearest-cloud distance of

less than 3 and 4 km over land and sea, respectively. After applying our bias correction the mean bias in the proximity of clouds is close to zero. Thus, the bias correction effectively mitigates biases due to 3D cloud effects.

4.2 Linear vs. non-linear bias correction

Building on the work by Massie et al. (2021) one of the guiding research questions was whether a non-linear approach based on interpretable machine learning techniques would improve upon a linear 3D cloud bias correction. To probe this question, we compare the performance of the non-linear random forest model to linear ridge regression (see Eq. 1). To train the linear model we used the same features and training and testing sets used for the random forest model development. The RMSEs for the linear model (OCO-2 lin. corr.) and non-linear model (OCO-2 corr.) are shown in Table 3. For QF = 0 land and sea observations the linear and non-linear model have similar performance, with the non-linear model allowing for a slightly lower RMSE. For QF = 1 the non-linear random forest reduces remaining biases further than the linear ridge regression, from 2.3 to 2.1 ppm over land and from 1.5 to 1.3 ppm over the sea.

4.3 Comparison to using dedicated cloud variables

A second question that we wanted to answer was whether additional variables from the OCO-2-retrieved state vector could improve the 3D cloud bias correction. As shown in Fig. 3, the four cloud variables (H3D, HC, CSNoiseRatio, nearest-cloud distance) were removed during the recursive-feature-elimination step, indicating that other variables from the state vector are more directly correlated with X_{CO_2} biases. To better understand how much of the model performance stems from the new set of features we performed a set of experiments. For the first experiment we trained a random forest using only the four cloud variables in addition to surface albedo, solar zenith angle, sensor zenith angle, and the difference between solar and sensor azimuth. The results are shown in Table 3 (OCO-2 cloud corr.). As ex-
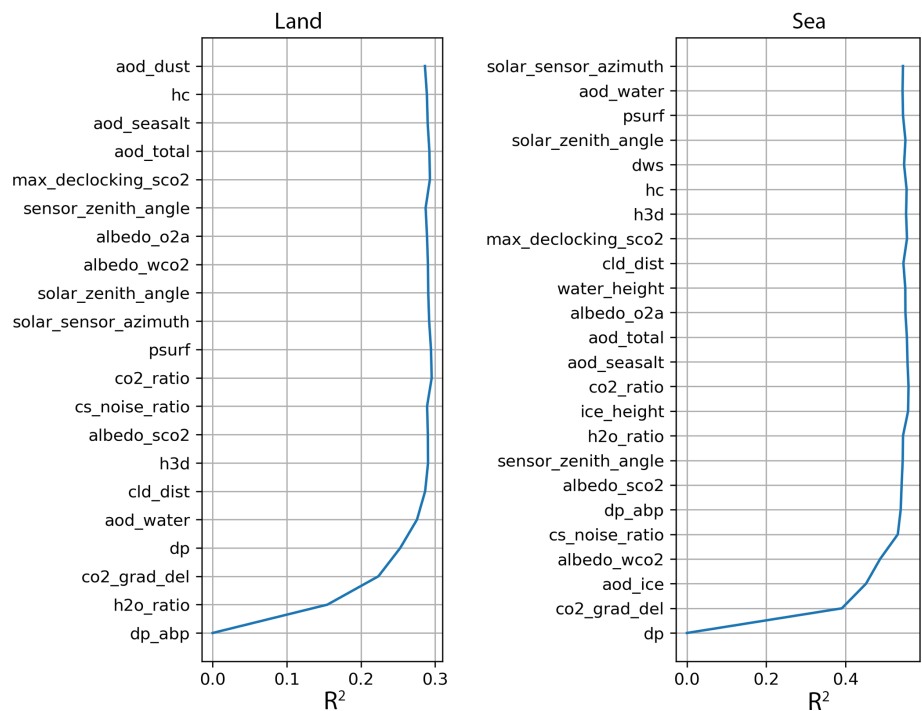
Figure 3. Feature ordering by importance as determined by recursive feature elimination. Features were removed from top to bottom, with the most important features on the bottom. The model performance for removing a given feature is indicated by R^2 calculated on the validation set. Please refer to p. 29 to 40 in Jet Propulsion Laboratory (2018) for a description of the individual features.

Table 3. RMSE of X_{CO_2} as determined by small-area analysis for the testing set (August 2018–July 2019). The RMSE is shown for the operational OCO-2 product (OCO-2), the proposed bias correction approach (OCO-2 corr.), a linear bias correction using the same features as the proposed approach (OCO-2 lin. corr.), and a random forest using dedicated cloud metrics (OCO-2 cloud corr.). The data are separated by high-quality data (QF = 0), low-quality data (QF = 1), and all data (QF = 0 + 1).

	Land X_{CO_2} (ppm)				Sea X_{CO_2} (ppm)			
	OCO-2 corr.	OCO-2 lin. corr.	OCO-2 cloud corr.	OCO-2	OCO-2 corr.	OCO-2 lin. corr.	OCO-2 cloud corr.	OCO-2
QF = 0	0.94	0.90	0.92	0.92	0.53	0.44	0.49	0.46
QF = 1	2.60	2.10	2.31	2.43	2.29	1.31	1.52	1.44
QF = 0 + 1	1.95	1.62	1.79	1.88	1.42	0.89	1.06	0.98

pected, using the cloud variables with the non-linear random forest model leads to worse performance than using the random forest with the features identified using the recursive feature elimination. One caveat of this experiment is that our bias correction approach, aimed at 3D cloud biases, might also make corrections for biases stemming from other effects (e.g., aerosols) that are independent of clouds and, thus, cannot be explained with cloud variables. Unfortunately, it is not possible to clearly separate various sources.

For the other experiment we combine the 3D cloud variables with the variables determined by the recursive feature elimination (dp_abp, co2_grad_del, h2o_ratio, dp, and aod_water for land and dp, co2_grad_del, aod_ice, and albedo_wco2 for sea) and compare the results to using only the features from the recursive feature elimination. If adding the 3D cloud variables would significantly reduce biases in X_{CO_2} further, it would indicate that the set of identified features is mostly correcting for biases unrelated to 3D cloud effects. In total we compare the model performance of four sets of features: the features determined by the recursive feature elimination in addition to (a) nearest-cloud distance; (b) CSNoiseRatio; (c) nearest-cloud distance, CSNoiseRatio, HC, and H3D; and (d) deltaT (see Tables 1 and 2). The last set of features serves as a control experiment where we quantify the effect of adding a random variable that is unrelated to 3D cloud effects to the set of chosen features. The results are shown in Table 4. For QF = 0 there are practically no differences for the four test cases compared to our chosen set of
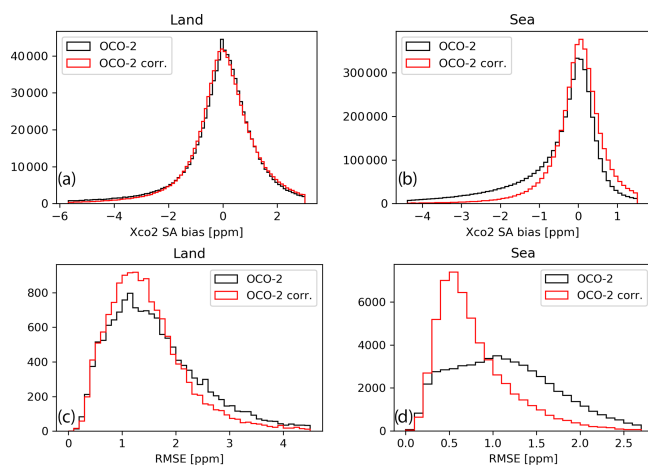
Figure 4. Reduction in non-physical variability in X_{CO_2} for OCO-2 and the proposed bias correction approach (OCO-2 corr.) for land **(a, c)** and sea **(b, d)** for QF = 0 and QF = 1 data from 2018 to 2019. **(a, b)** Distribution of biases from individual soundings, **(c, d)** distribution of standard deviation for individual small areas.

features. For sea QF = 1 data the best set of features is (c), which reduces the RMSE from 1.31 to 1.25 ppm. Overall, the addition of 3D cloud variables (a, b, c) allows the models to lower the RMSE further compared to our proposed model; however, the improvements are only marginal. This indicates that the set of chosen features in our bias correction model accounts for the majority of 3D cloud biases in X_{CO_2}. Further evidence for this is shown in Fig. 5 and is presented in the next section with an independent comparison to TCCON.

4.4 Comparison to TCCON

We further compare bias-corrected X_{CO_2} to TCCON. TCCON observations have low uncertainties and are used to validate OCO-2-retrieved X_{CO_2}. However, they can only provide point measurements and are non-uniformly distributed, with most TCCON sites over land and in the Northern Hemisphere. For our comparison we consider coinciding observations of OCO-2 and TCCON for the period of the testing set (August 2018–July 2019). This results in 1768 (QF = 0: 7459; QF = 1: 2794) matches over land and 1305 (QF = 0: 2165; QF = 1: 1111) matches over sea. Note that our bias correction model was trained without taking TCCON observations into consideration, while OCO-2 takes OCO-2–TCCON biases explicitly into consideration for its linear bias correction and filtering and to calculate global offsets. Thus, comparisons between OCO-2 and TCCON are not independent.

Table 5 shows the mean and standard deviation of differences between OCO-2 and TCCON and after we apply our bias correction (OCO-2 corr. – TCCON) for QF = 0 and QF = 1. Over land and sea the bias correction reduces the standard deviation between OCO-2 and TCCON for QF = 0

and QF = 1. For observations over sea the bias-corrected X_{CO_2} exhibits a systematic positive offset compared to TCCON of about 0.7 ppm. The systematic offset could be addressed by recalculating the scaling factor used for retrievals over sea in OCO-2. However, there are only few TCCON stations that can provide comparisons for those data, and these stations are not equally distributed over the ocean.

To better understand how the bias correction addresses 3D cloud biases as compared to TCCON, Fig. 6 shows X_{CO_2} biases vs. nearest-cloud distance. For land and sea there are negative biases in OCO-2 in the proximity of clouds (Fig. 6a and c). Interestingly, there is a positive bias for OCO-2 sea data when no clouds are close to OCO-2 soundings (> 2 km) that likely stems from OCO-2 incorporating a multi-model mean in its bias correction in addition to TCCON. After applying our bias correction, X_{CO_2} biases over land show a reduced dependence on nearest-cloud distance (Fig. 6b). For sea, the bias correction pushed X_{CO_2} up by roughly 0.5 ppm in the proximity of clouds, resulting in a uniform positive bias of 0.7 ppm independent of cloud distance (Fig. 6d). Thus, the bias correction removed the dependency of X_{CO_2} biases on nearest-cloud distance but did not address the overall offset present in OCO-2.

5 Discussion

5.1 Model interpretation

To better understand how the model utilizes the input features to calculate the bias correction we show the modeled biases with respect to the individual features in Fig. 7. Overall, the bias–feature relationship is non-linear for most features over the complete state space but linear over part of the state space. This explains the lower model performance of the linear model we compared to in Sect. 4.2 over the complete state space (QF = 0 + 1) and the only marginal improvement compared to QF = 0 data. Differences between retrieved surface pressure and a reference surface pressure (dp, dp_abp) show a positive correlation with X_{CO_2} biases. When the operationally retrieved surface pressure is underestimated, X_{CO_2} is underestimated as well. The ratio of the retrieved H_2O column from the WCO_2 band to that from the SCO_2 band (h2o_ratio), for soundings over land (Fig. 7b), is independent of X_{CO_2} biases for ratios of less than 1 and has a strong negative correlation for ratios above 1. A ratio of 1.05 corresponds on average to an X_{CO_2} bias of -1.5 ppm. The difference between the retrieved CO_2 profile and the a priori profile (co2_grad_del) shows mostly a positive correlation for negative values (surface CO_2 is underestimated compared to CO_2 higher up in the atmosphere) and a negative correlation for positive values. This indicates that 3D cloud effects challenge the accurate retrieval of the X_{CO_2} profile. The sensitivity of X_{CO_2} biases to changes in co2_grad_del is approximately twice as strong over sea compared to land (see Fig. 7c
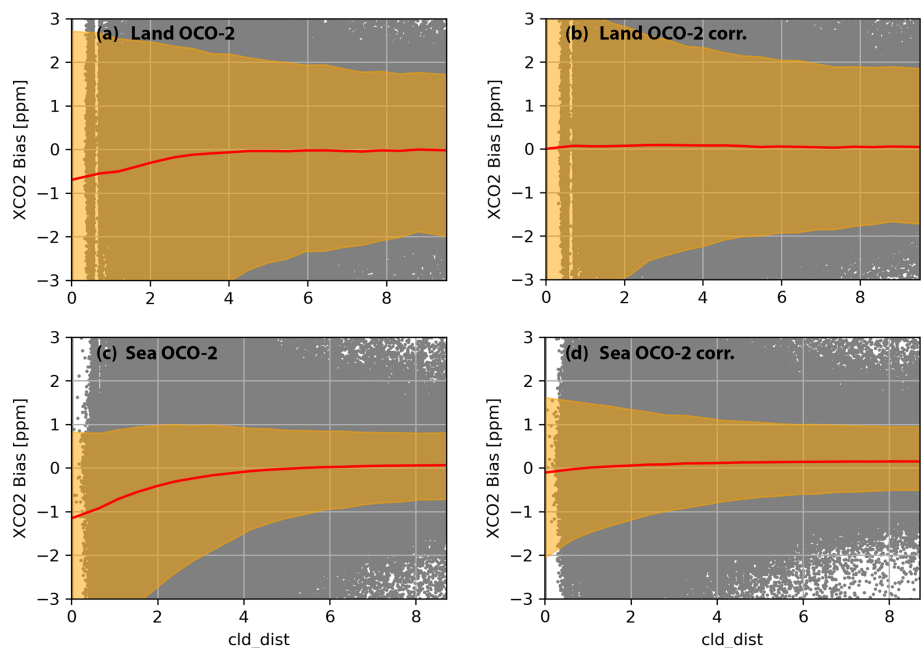
Figure 5. X_{CO_2} bias vs. cloud distance for OCO-2 soundings over land **(a)**, soundings over land corrected by our proposed method **(b)**, OCO-2 soundings over sea **(c)**, and soundings over sea that are corrected **(d)** for QF = 0 and QF = 1 data from 2018 to 2019. The 5th and 95th percentiles are indicated by the yellow shaded area, the mean is shown by a red line, and individual comparisons are shown by gray dots.

Table 4. RMSE of X_{CO_2} as determined by small-area analysis for the testing set (August 2018 –July 2019). The RMSE is shown for the proposed bias correction approach (OCO-2 corr.) and using the same approach but with additional features. In addition to the variables determined by the recursive feature elimination, (a) shows nearest-cloud distance; (b) shows CSNoiseRatio; (c) shows nearest-cloud distance, CSNoiseRatio, HC, and H3D; and (d) shows deltaT.

	Land X_{CO_2} (ppm)					Sea X_{CO_2} (ppm)				
	OCO-2 corr.	(a)	(b)	(c)	(d)	OCO-2 corr.	(a)	(b)	(c)	(d)
QF = 0	0.90	0.90	0.90	0.90	0.90	0.44	0.43	0.43	0.42	0.44
QF = 1	2.10	2.09	2.10	2.08	2.10	1.31	1.29	1.28	1.25	1.28
QF = 0 + 1	1.62	1.62	1.62	1.61	1.62	0.89	0.87	0.86	0.84	0.87

and f). This feature cannot be exclusively linked to 3D cloud effects since it is one of the most important features for the operational bias correction of OCO-2. The retrieved extinction optical depth of cloud water (aod_water) shows a mostly negative linear correlation with a X_{CO_2} bias of −2 ppm for an extinction optical depth of 0.1. The retrieved extinction optical depth of cloud ice (aod_ice) is negatively correlated with X_{CO_2} biases. Finally, the surface albedo in the weak CO_2 band (albedo_wco2) has mostly no dependence on X_{CO_2} biases for most of its range but shows some negative correlation with biases for brighter surfaces. Note that our bias correction is applied in addition to the bias correction that has already been performed in the operational OCO-2 retrieval. While the operational OCO-2 bias correction does not explicitly account for 3D cloud biases it might implicitly mitigate such biases with its linear bias correction (since the opera-

tional bias correction variable dp is correlated with nearest-cloud distance; see the red line in Fig. 2b).

To understand why some variables of the OCO-2-retrieved state vector are correlated with 3D cloud biases it is important to remember that the operational retrieval, based on optimal estimation, tries to match the observed radiances with a forward radiative transfer model. However, while the observed radiances can be perturbed by 3D cloud effects, the forward model tries to match those radiances with an independent pixel approximation that does not physically include 3D cloud effects. In particular the 3D cloud effect enhances, or brightens, the radiances as compared to no clouds being present. To compensate for this brightening the forward model decreases the retrieved surface pressure (reduction in dp and dp_abp), increases the optical depth of cloud water (aod_water), and increases the surface albedo in the WCO2

Table 5. Mean and standard deviation of bias in X_{CO_2} compared to TCCON observations for the testing set (August 2018–July 2019). The comparison for the operational OCO-2 product is indicated by OCO-2 – TCCON and the proposed random forest approach by OCO-2 corr. – TCCON.

	Land X_{CO_2} (ppm)		Sea X_{CO_2} (ppm)	
	OCO-2 – TCCON	OCO-2 corr. – TCCON	OCO-2 – TCCON	OCO-2 corr. – TCCON
QF = 0	-0.05 ± 1.24	-0.16 ± 1.21	0.57 ± 0.74	0.67 ± 0.69
QF = 1	-1.7 ± 4.21	0.45 ± 2.77	-1.01 ± 1.83	0.59 ± 1.34
QF = 0 + 1	0.47 ± 2.42	-0.23 ± 1.74	0.06 ± 1.40	0.69 ± 0.97
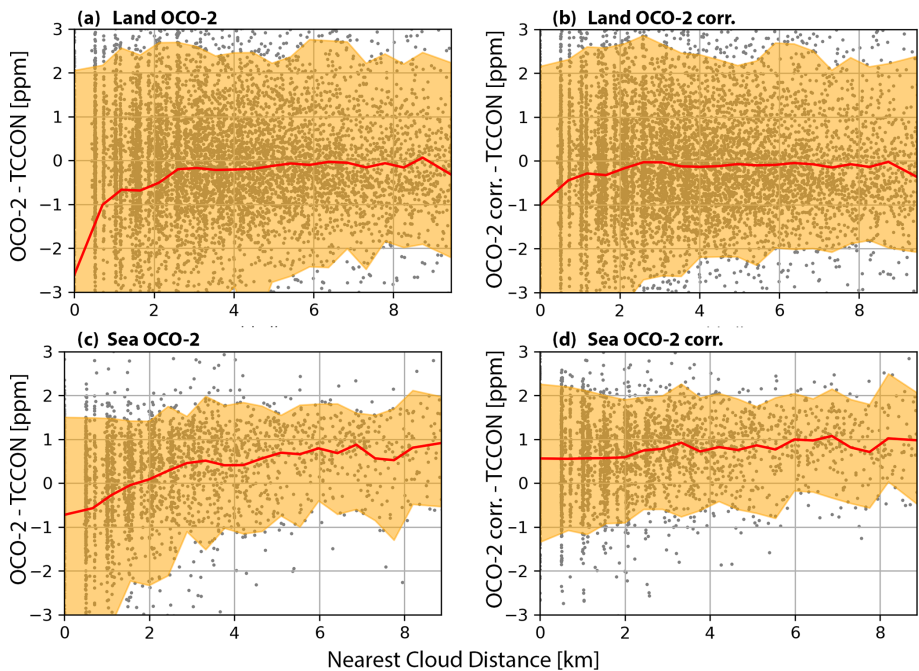
Figure 6. X_{CO_2} bias vs. cloud distance of OCO-2 over land **(a)**, OCO-2-corrected **(b)**, OCO-2 over sea **(c)**, and OCO-2-corrected **(d)** for QF = 0 and QF = 1 data from 2018 to 2019. The 5th and 95th percentiles are indicated by the yellow shaded area, the mean is shown with a red line, and individual comparisons are shown with gray dots.

band. These relationships are shown empirically in Fig. 7. As shown in Fig. 2 of Massie et al. (2021), the spectral signature of the 3D cloud effect (the optical depth structure of the radiative perturbation of the 3D effect) differs from the spectral signatures of perturbations in surface pressure, surface reflectivity, aerosol, and X_{CO_2}. Figure 2 illustrates that a decrease in surface pressure and X_{CO_2} and an increase in surface reflectance will increase the observed radiance. In order to provide for extra radiance enhancement in the cloud-brightened observed radiance, a variety of state variable adjustments (and their unique spectral contributions) are utilized by the retrieval to bring forward model radiances in agreement with the observed radiances. The relationship of 3D cloud biases to surface pressure differences and surface albedo is likely due to a combination of physically based 3D cloud radiative effects and operational-retrieval-algorithmic considerations.

A further look at the relative importance of the model features shows dp_abp as being the most important feature for land and dp for sea observations. Over land dp_abp is followed by dp, h2o_ratio, co2_grad_del, and aod_water. Over sea dp is followed by co2_grad_del, aod_ice, and albedo_wco2 (see Fig. 8). The feature importance was calculated as the normalized total reduction in mean square error brought by an individual feature; i.e., if we were to omit dp from our model as a feature the bias correction would be less effective than if we were to omit co2_grad_del.

5.2 Regional biases

To further understand regional impacts of our bias correction we calculate biases, as identified by our model, for soundings from 2014 to 2019 and averaged results over $2° \times 2°$ cells (see Fig. 9); i.e., in applying the proposed bias correction, the results shown in Fig. 9 are subtracted from OCO-2 X_{CO_2}.
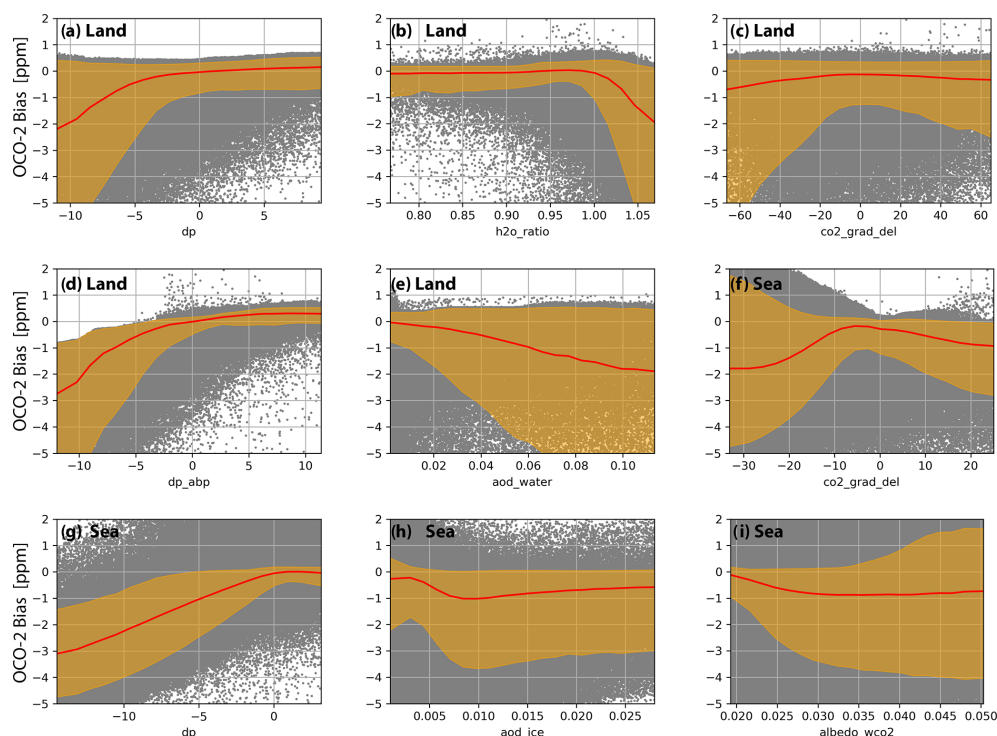
Figure 7. Bias identified by correction by the proposed model (OCO-2 bias) with respect to its features: dp **(a)**, h2o_ratio **(b)**, co2_grad_del **(c)**, dp_abp **(d)**, aod_water **(e)** over land and co2_grad_del **(f)**, dp **(g)**, aod_ice **(h)**, and albedo_wco2 **(i)** over sea for QF = 0 and QF = 1 data from 2018 to 2019. The 5th and 95th percentiles are indicated by the yellow shaded area, the mean is shown with a red line, and individual comparisons are shown with gray dots. The scale of the x axis is different for each plot. Please refer to Sect. 3.4 for a description of the individual features.
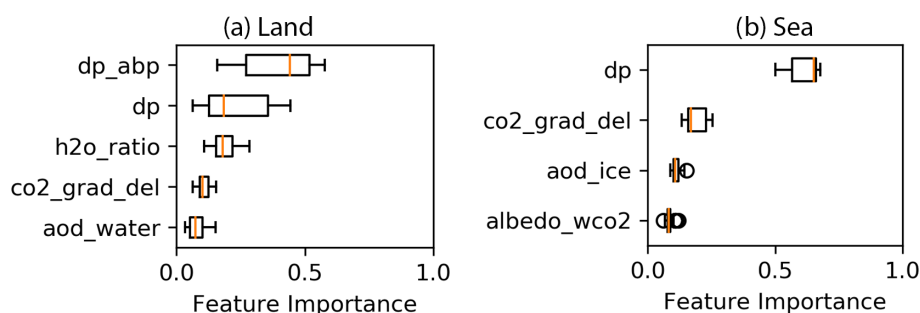
Figure 8. Feature importance for the bias correction model. Feature importance is shown for land **(a)** and sea **(b)** observations. The model was trained using the training set with QF = 0 and QF = 1 data. Please refer to Sect. 3.4 for a description of the individual features.

Since using soundings only from the testing set leads to many areas with no data, we used all available data (2014–2019) for this visualization. Over land negative biases (i.e., X_{CO_2} from OCO-2 is underestimated) are present north of 45° in America, Europe, and Asia, averaging −0.3 ppm. Around the tropics within ±10° of the Equator, average biases are near −0.3 ppm as well. Positive biases are most dominant over the deserts of northern Africa and Saudi Arabia. Over sea biases are more equally distributed than over land. When comparing the regional biases to a map of nearest-cloud distance (see Fig. 10) there is overlap between negative biases and

areas dominated by clouds (correlation coefficient between nearest-cloud distance and OCO-2 bias is $R = 0.3$).

5.3 Effect of bias correction on true CO_2 enhancements

As discussed in Sect. 3.1 we use the small-area analysis as a truth proxy to develop our model. This assumes that CO_2 is well mixed and constant over short spatial scales (< 100 km). However, this assumption is violated for strong CO_2 emitters such as power plants. Even though these strong emitters are rare in the data and likely do not influence the bias correc-
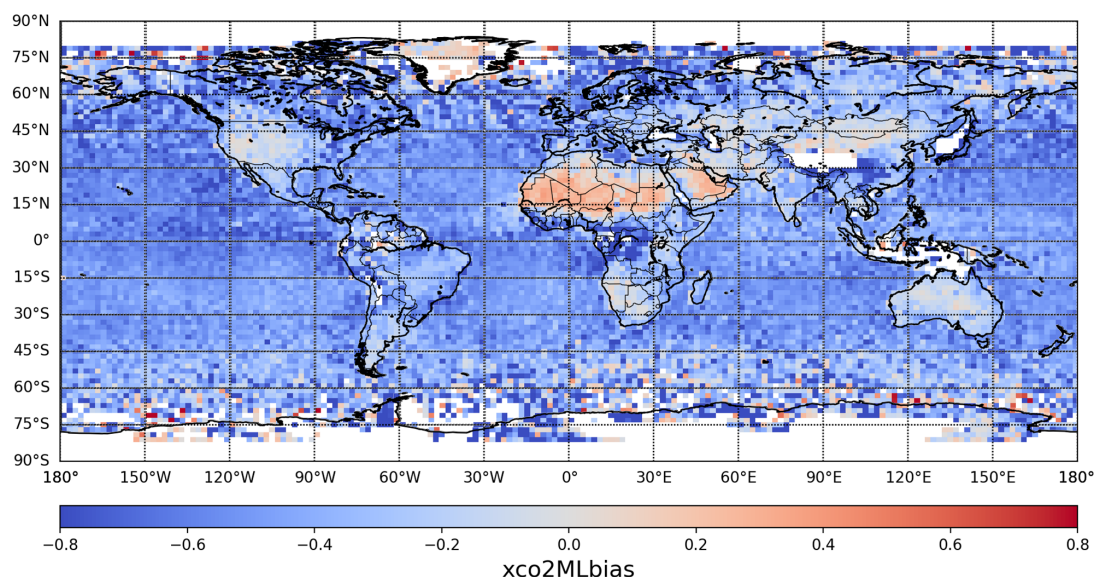
Figure 9. Biases in X_{CO_2} identified by our model. Biases are averaged over $2° \times 2°$ for all soundings (2014 to 2019; QF = 0 and QF = 1). Negative biases are shown in blue, positive biases in red, and "no data" in white.
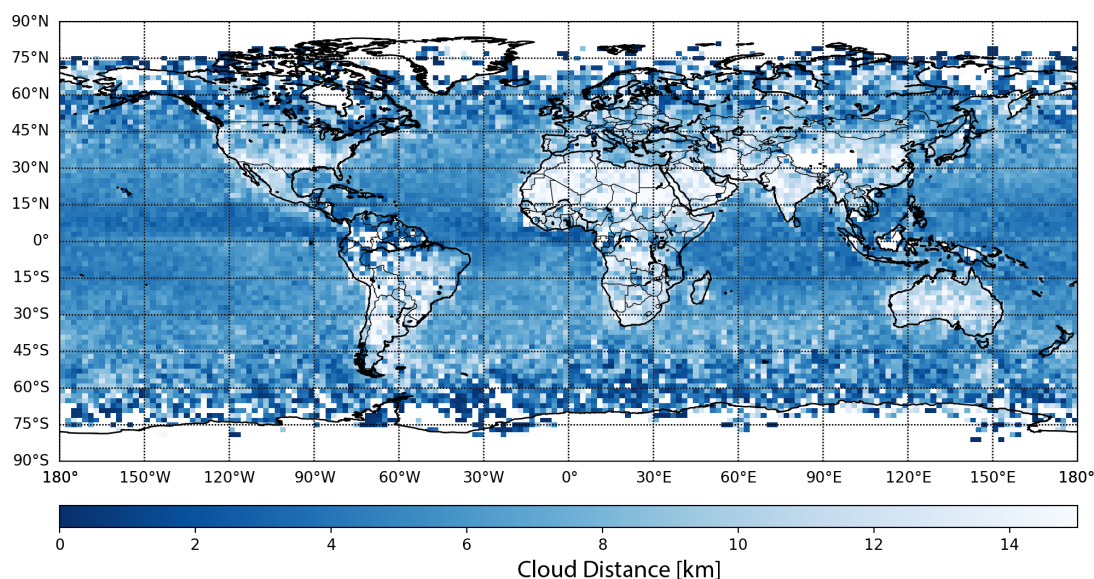
Figure 10. Nearest-cloud distance derived from MODIS. Nearest-cloud distances are averaged over $2° \times 2°$ for all matched soundings (2014 to 2019; QF = 0 and QF = 1). Darker blues indicate closer clouds; "no data" is shown in white.

tion model, there is a risk that the model would "correct", i.e., remove, real local CO_2 enhancements. To confirm that real CO_2 enhancements are still present after the proposed bias correction, we compare OCO-2-retrieved and OCO-2-corrected X_{CO_2} from three OCO-2 overpasses over large coal power plants (see Fig. 11) that have been used in a previous study (Nassar et al., 2017). The CO_2 enhancements of the retrieved and corrected X_{CO_2} for the three overpasses (the singular spikes in X_{CO_2} in the middle of the graphs) agree closely and demonstrate that the *bias correction does not er-*

roneously remove true CO_2 enhancements from the OCO-2 data record.

6 Future work and conclusion

6.1 Future work

The developed bias correction approach is aimed at mitigating 3D cloud biases in OCO-2 but could readily be expanded to a more general bias correction. Future research will need
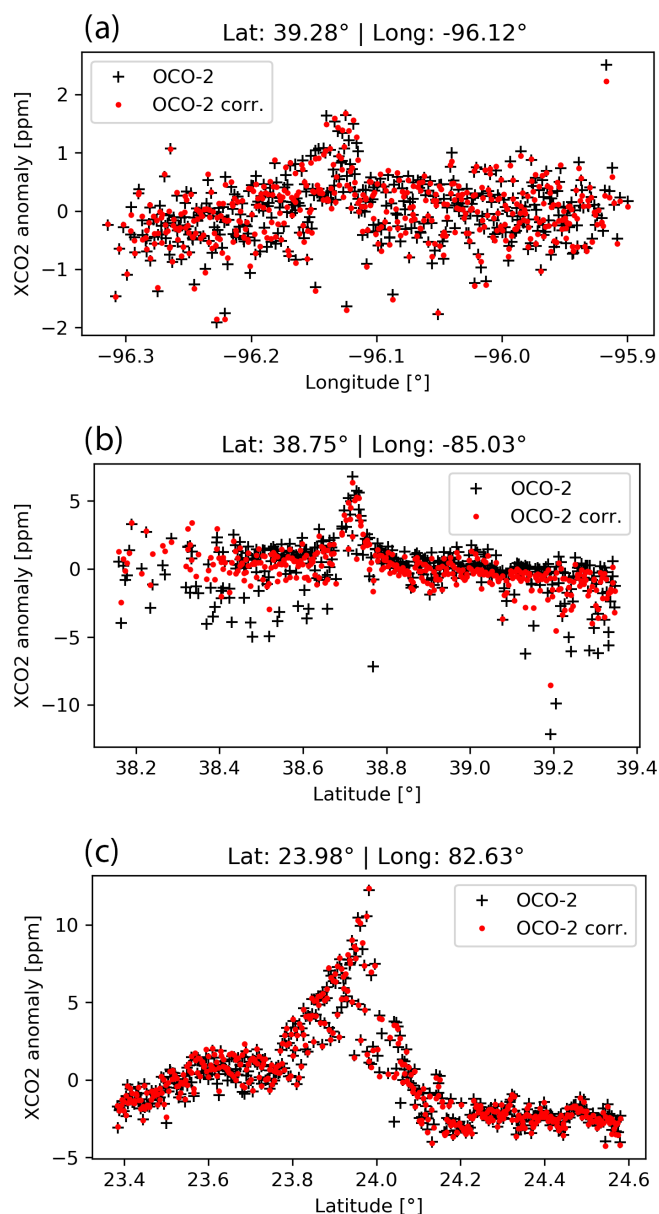
Figure 11. X_{CO_2} anomalies for OCO-2 and bias-corrected OCO-2 retrievals in the proximity of coal power plants. Power plant **(a)** Westar at lat 39.28°, long −96.12°, on 4 December 2015; **(b)** Ghent at lat 38.75°, long −85.03°, on 13 August 2015; and **(c)** Sasan at lat 23.98°, long −82.63°, on 23 October 2014. Anomaly is calculated by subtracting the mean.

to show how far the approach used in this research (determining the bias correction solely from small-area biases) will work for correcting previously uncorrected X_{CO_2} (the "raw" X_{CO_2} from the operational retrieval). For such a correction a two-step approach might be necessary that combines a global (comparison to TCCON) and local (small-area analysis) bias correction approach. However, developing such an approach

would be challenged by the sparse coverage of TCCON stations.

The operational bias correction used for OCO-2 is aimed at QF = 0 data. This is highlighted by the significant reduction in X_{CO_2} biases our correction was able to achieve in QF = 1 data, while improvements in QF = 0 data were small. Filtering out low-quality data is a simple approach to improve the overall quality of the OCO-2 X_{CO_2} retrieval. However, it leaves certain areas with too few samples, most notably the tropics (due to clouds); higher latitudes (due to large solar zenith angles); and around Brazil, Bolivia, and Paraguay (due to the South Atlantic Anomaly). Improving the bias correction of future OCO-2 versions that allow for less restrictive filtering would benefit applications that rely on those data.

Finally, one could expand the approach taken here, developing one model for land and one for sea data, to have multiple models for land and sea to better capture the diverse causes for biases in X_{CO_2} across Earth; for example, different types of aerosols dominate different areas and might lead to specific biases in different regions or seasons. Such a location-based bias correction could also be expanded to a location-based filtering approach that would, for example, allow less restrictive filtering at higher latitudes (Mendonca et al., 2021; Jacobs et al., 2020) to have more of those soundings pass the filter and be available for scientific inquiry. A key challenge of such an approach will be validation due to the limited number of available TCCON stations.

6.2 Conclusion

We identified five variables from the state vector for OCO-2 retrievals over land (dp, dp_abp, h2o_ratio, co2_grad_del, aod_water) and four variables over sea (dp, co2_grad_del, aod_ice, albedo_wco2) that are used in a machine learning model that allows 3D cloud biases to be mitigated in OCO-2-retrieved X_{CO_2}. We demonstrate that this machine learning model does not erroneously remove true CO_2 power plant enhancements from the OCO-2 data record. All variables are by-products of the operational retrieval used by OCO-2, which simplifies their inclusion for bias correction in future versions of the operational product. The proposed nonlinear bias correction is based on a random forest approach and is able to reduce the RMSE from 1.95 to 1.62 ppm over land and 1.42 to 0.89 ppm over sea for QF = 0 and QF = 1 data on an independent testing set. We demonstrated a systematic approach to correct for biases in optimal estimation retrievals. Namely, (1) find a physical variable that is well understood and correlated with the cause of the bias (in our case "nearest-cloud distance"), (2) identify elements from the retrieved state vector and other retrieval products that show a dependence on the variable from step (1) in addition to other variables that have a physical connection to the bias, (3) use recursive feature elimination to identify which subset of the elements identified in (2) should be used for the bias cor-

rection, and (4) use a simple explainable machine learning model to map the features identified in (3) to the biases and correct for them.

References

Breiman, L.: Random forests, Mach. Learn., 45, 5–32, 2001.

Chen, S., Natraj, V., Zeng, Z.-C., and Yung, Y. L.: Machine learning-based aerosol characterization using OCO-2 O_2 A-band observations, J. Quant. Spectrosc. Ra., 279, 108049, https://doi.org/10.1016/j.jqsrt.2021.108049, 2022.

Crisp, D., Atlas, R. M., Breon, F. M., Brown, L. R., Burrows, J. P., Ciais, P., Connor, B. J., Doney, S. C., Fung, I. Y., Jacob, D. J., Miller, C. E., O'Brien, D., Pawson, S., Randerson, J. T., Rayner, P., Salawitch, R. J., Sander, S. P., Sen, B., Stephens, G. L., Tans, P. P., Toon, G. C., Wennberg, P. O., Wofsy, S. C., Yung, Y. L., Kuang, Z., Chudasama, B., Sprague, G., Weiss, B., Pollock, R., Kenyon, D., and Schroll, S.: The Orbiting Carbon Observatory (OCO) mission, Adv. Space Res., 34, 700–709, https://doi.org/10.1016/j.asr.2003.08.062, 2004.

Cronk, H.: OCO-2/MODIS Collocation Products User Guide, Version 3, ftp://ftp.cira.colostate.edu/ftp/TTaylor/publications/ (last access: 13 March 2023), 2018.

Dubey, M., Henderson, B., Green, D., Butterfield, Z., Keppel-Aleks, G., Allen, N., Blavier, J. F., Roehl, C., Wunch, D., and Lindenmaier, R.: TCCON data from Manaus (BR), Release GGG2014R0, CaltechDATA [data set], https://doi.org/10.14291/tccon.ggg2014.manaus01.R0/1149274, 2014a.

Dubey, M., Lindenmaier, R., Henderson, B., Green, D., Allen, N., Roehl, C., Blavier, J. F., Butterfield, Z., Love, S., Hamelmann, J., and Wunch, D.: TCCON data from Four Corners (US), Release GGG2014R0, CaltechDATA [data set], https://doi.org/10.14291/tccon.ggg2014.fourcorners01.R0/1149272, 2014b.

Eldering, A., O'Dell, C. W., Wennberg, P. O., Crisp, D., Gunson, M. R., Viatte, C., Avis, C., Braverman, A., Castano, R., Chang, A., Chapsky, L., Cheng, C., Connor, B., Dang, L., Doran, G., Fisher, B., Frankenberg, C., Fu, D., Granat, R., Hobbs, J., Lee, R. A. M., Mandrake, L., McDuffie, J., Miller, C. E., Myers, V., Natraj, V., O'Brien, D., Osterman, G. B., Oyafuso, F., Payne, V. H., Pollock, H. R., Polonsky, I., Roehl, C. M., Rosenberg, R., Schwandner, F., Smyth, M., Tang, V., Taylor, T. E., To, C., Wunch, D., and Yoshimizu, J.: The Orbiting Carbon Observatory-2: first 18 months of science data products, Atmos. Meas. Tech., 10, 549–563, https://doi.org/10.5194/amt-10-549-2017, 2017.

Eldering, A., Taylor, T. E., O'Dell, C. W., and Pavlick, R.: The OCO-3 mission: measurement objectives and expected performance based on 1 year of simulated data, Atmos. Meas. Tech., 12, 2341–2370, https://doi.org/10.5194/amt-12-2341-2019, 2019.

Emde, C., Yu, H., Kylling, A., van Roozendael, M., Stebel, K., Veihelmann, B., and Mayer, B.: Impact of 3D cloud structures on the atmospheric trace gas products from UV–Vis sounders – Part 1: Synthetic dataset for validation of trace gas retrieval algorithms, Atmos. Meas. Tech., 15, 1587–1608, https://doi.org/10.5194/amt-15-1587-2022, 2022.

Evans, K. F.: The spherical harmonics discrete ordinate method for three-dimensional atmospheric radiative transfer, J. Atmos. Sci., 55, 429–446, https://doi.org/10.1175/1520-0469(1998)055<0429:TSHDOM>2.0.CO;2, 1998.

Hoerl, A. E. and Kennard, R. W.: Ridge regression: Biased estimation for nonorthogonal problems, Technometrics, 12, 55–67, 1970a.

Hoerl, A. E. and Kennard, R. W.: Ridge regression: applications to nonorthogonal problems, Technometrics, 12, 69–82, 1970b.

Iraci, L., Podolske, J., Hillyard, P., Roehl, C., Wennberg, P. O., Blavier, J. F., Landeros, J., Allen, N., Wunch, D., Zavaleta, J., Quigley, E., Osterman, G. B., Barrow, E., and Barney, J.: TC-

CON data from Indianapolis (US), Release GGG2014R0, CaltechDATA [data set], https://doi.org/10.14291/tccon.ggg2014.indianapolis01.R0/1149164, 2014.

Iraci, L. T., Podolske, J., Hillyard, P. W., Roehl, C., Wennberg, P. O., Blavier, J. F., Allen, N., Wunch, D., Osterman, G. B., and Albertson, R.: TCCON data from Edwards (US), Release GGG2014R1, CaltechDATA [data set], https://doi.org/10.14291/tccon.ggg2014.edwards01.R1/1255068, 2016.

Jacobs, N., Simpson, W. R., Wunch, D., O'Dell, C. W., Osterman, G. B., Hase, F., Blumenstock, T., Tu, Q., Frey, M., Dubey, M. K., Parker, H. A., Kivi, R., and Heikkinen, P.: Quality controls, bias, and seasonality of CO_2 columns in the boreal forest with Orbiting Carbon Observatory-2, Total Carbon Column Observing Network, and EM27/SUN measurements, Atmos. Meas. Tech., 13, 5033–5063, https://doi.org/10.5194/amt-13-5033-2020, 2020.

Jet Propulsion Laboratory: Orbiting Carbon Observatory–2 (OCO-2) Data Product User's Guide, Operational L1 and L2 Data Versions 8 and Lite File Version 9, https://docserver.gesdisc.eosdis.nasa.gov/public/project/OCO/OCO2_DUG.pdf (last access: 13 March 2023), 2018.

Kiel, M., O'Dell, C. W., Fisher, B., Eldering, A., Nassar, R., MacDonald, C. G., and Wennberg, P. O.: How bias correction goes wrong: measurement of X_{CO_2} affected by erroneous surface pressure estimates, Atmos. Meas. Tech., 12, 2241–2259, https://doi.org/10.5194/amt-12-2241-2019, 2019.

Kylling, A., Emde, C., Yu, H., van Roozendael, M., Stebel, K., Veihelmann, B., and Mayer, B.: Impact of 3D cloud structures on the atmospheric trace gas products from UV–Vis sounders – Part 3: Bias estimate using synthetic and observational data, Atmos. Meas. Tech., 15, 3481–3495, https://doi.org/10.5194/amt-15-3481-2022, 2022.

Liang, L., Di Girolamo, L., and Platnick, S.: View-angle consistency in reflectance, optical thickness and spherical albedo of marine water-clouds over the northeastern Pacific through MISR-MODIS fusion, Geophys. Res. Lett., 36, L09811, https://doi.org/10.1029/2008GL037124, 2009.

Massie, S., Sebastian, S., Eldering, A., and Crisp, D.: Observational evidence of 3-D cloud effects in OCO-2 CO_2 retrievals, J. Geophys. Res.-Atmos., 122, 7064–7085, https://doi.org/10.1002/2016JD026111, 2017.

Massie, S., Cronk, H., Merrelli, A., Schmidt, K. S., Chen, H., and Baker, D.: 3D cloud metrics for OCO-2 observations, Zenodo [data set], https://doi.org/10.5281/zenodo.4008764, 2020.

Massie, S., Cronk, H., Merrelli, A., Schmidt, S., and Mauceri, S.: Insights into 3D cloud radiative transfer for OCO-2, Atmos. Meas. Tech. Discuss. [preprint], https://doi.org/10.5194/amt-2022-323, in review, 2022.

Massie, S. T., Cronk, H., Merrelli, A., O'Dell, C., Schmidt, K. S., Chen, H., and Baker, D.: Analysis of 3D cloud effects in OCO-2 XCO2 retrievals, Atmos. Meas. Tech., 14, 1475–1499, https://doi.org/10.5194/amt-14-1475-2021, 2021.

Mendonca, J., Nassar, R., O'Dell, C. W., Kivi, R., Morino, I., Notholt, J., Petri, C., Strong, K., and Wunch, D.: Assessing the feasibility of using a neural network to filter Orbiting Carbon Observatory 2 (OCO-2) retrievals at northern high latitudes, Atmos. Meas. Tech., 14, 7511–7524, https://doi.org/10.5194/amt-14-7511-2021, 2021.

Merrelli, A., Bennartz, R., O'Dell, C. W., and Taylor, T. E.: Estimating bias in the OCO-2 retrieval algorithm caused by 3-D radiation

scattering from unresolved boundary layer clouds, Atmos. Meas. Tech., 8, 1641–1656, https://doi.org/10.5194/amt-8-1641-2015, 2015.

Nassar, R., Hill, T. G., McLinden, C. A., Wunch, D., Jones, D. B. A., and Crisp, D.: Quantifying CO_2 Emissions From Individual Power Plants From Space, Geophys. Res. Lett., 44, 10045–10053, https://doi.org/10.1002/2017GL074702, 2017.

OCO-2 Science Team, Gunson, M., and Eldering, A.: OCO-2 Level 2 bias-corrected XCO2 and other select fields from the full-physics retrieval aggregated as daily files, Retrospective processing V10r, Goddard Earth Sciences Data and Information Services Center (GES DISC) [data set], Greenbelt, MD, USA, https://doi.org/10.5067/E4E140XDMPO2, 2020.

O'Dell, C. W., Eldering, A., Wennberg, P. O., Crisp, D., Gunson, M. R., Fisher, B., Frankenberg, C., Kiel, M., Lindqvist, H., Mandrake, L., Merrelli, A., Natraj, V., Nelson, R. R., Osterman, G. B., Payne, V. H., Taylor, T. E., Wunch, D., Drouin, B. J., Oyafuso, F., Chang, A., McDuffie, J., Smyth, M., Baker, D. F., Basu, S., Chevallier, F., Crowell, S. M. R., Feng, L., Palmer, P. I., Dubey, M., García, O. E., Griffith, D. W. T., Hase, F., Iraci, L. T., Kivi, R., Morino, I., Notholt, J., Ohyama, H., Petri, C., Roehl, C. M., Sha, M. K., Strong, K., Sussmann, R., Te, Y., Uchino, O., and Velazco, V. A.: Improved retrievals of carbon dioxide from Orbiting Carbon Observatory-2 with the version 8 ACOS algorithm, Atmos. Meas. Tech., 11, 6539–6576, https://doi.org/10.5194/amt-11-6539-2018, 2018.

Okata, M., Nakajima, T., Suzuki, K., Inoue, T., Nakajima, T., and Okamoto, H.: A study on radiative transfer effects in 3-D cloudy atmosphere using satellite data, J. Geophys. Res.-Atmos., 122, 443-468, https://doi.org/10.1002/2016JD025441, 2017.

Payne, V. H., Drouin, B. J., Oyafuso, F., Kuai, L., Fisher, B. M., Sung, K., Nemchick, D., Crawford, T. J., Smyth, M., and Crisp, D.: Absorption coefficient (ABSCO) tables for the Orbiting Carbon Observatories: version 5.1, J. Quant. Spectrosc. Ra., 255, 107217, https://doi.org/10.1016/j.jqsrt.2020.107217, 2020.

Rodgers, C. D.: Inverse methods for atmospheric sounding: theory and practice, World Scientific, ISBN 9814498688, 2000.

Toon, G. C. and Wunch, D.: A stand-alone a priori profile generation tool for GGG2014 release, GGG2014.R0, CaltechDATA [data set], https://doi.org/10.14291/tccon.ggg2014.priors.R0/1221661, 2014.

Total Carbon Column Observing Network (TCCON) Team: 2014 TCCON Data Release, Version GGG2014, CaltechDATA [data set], https://doi.org/10.14291/TCCON.GGG2014, 2017.

Wennberg, P. O., Wunch, D., Yavin, Y., Toon, G. C., Blavier, J. F., Allen, N., and Keppel-Aleks, G.: TCCON data from Jet Propulsion Laboratory (US), 2007, Release GGG2014R0, CaltechDATA [data set], https://doi.org/10.14291/tccon.ggg2014.jpl01.R0/1149163, 2014a.

Wennberg, P. O., Roehl, C., Wunch, D., Toon, G. C., Blavier, J. F., Washenfelder, R. a., Keppel-Aleks, G., Allen, N., and Ayers, J.: TCCON data from Park Falls (US), Release GGG2014R0, CaltechDATA [data set], https://doi.org/10.14291/tccon.ggg2014.parkfalls01.R0/1149161, 2014b.

Wennberg, P. O., Wunch, D., Roehl, C., Blavier, J. F., Toon, G. C., and Allen, N.: TCCON data from Caltech (US), Release GGG2014R1, CaltechDATA [data set], https://doi.org/10.14291/tccon.ggg2014.pasadena01.R1/1182415, 2015.

Wennberg, P. O., Roehl, C., Blavier, J. F., Wunch, D., Landeros, J., and Allen, N.: TCCON data from Jet Propulsion Laboratory (US), 2011, Release GGG2014R1, CaltechDATA [data set], https://doi.org/10.14291/tccon.ggg2014.jpl02.R1/1330096, 2016a.

Wennberg, P. O., Wunch, D., Roehl, C., Blavier, J. F., Toon, G. C., Allen, N., Dowell, P., Teske, K., Martin, C., and Martin, J.: TCCON data from Lamont (US), Release GGG2014R1, CaltechDATA [data set], https://doi.org/10.14291/tccon.ggg2014.lamont01.R1/1255070, 2016b.

Wunch, D., Toon, G. C., Wennberg, P. O., Wofsy, S. C., Stephens, B. B., Fischer, M. L., Uchino, O., Abshire, J. B., Bernath, P., Biraud, S. C., Blavier, J.-F. L., Boone, C., Bowman, K. P., Browell, E. V., Campos, T., Connor, B. J., Daube, B. C., Deutscher, N. M., Diao, M., Elkins, J. W., Gerbig, C., Gottlieb, E., Griffith, D. W. T., Hurst, D. F., Jiménez, R., Keppel-Aleks, G., Kort, E. A., Macatangay, R., Machida, T., Matsueda, H., Moore, F., Morino, I., Park, S., Robinson, J., Roehl, C. M., Sawa, Y., Sherlock, V., Sweeney, C., Tanaka, T., and Zondlo, M. A.: Calibration of the Total Carbon Column Observing Network using aircraft profile data, Atmos. Meas. Tech., 3, 1351–1362, https://doi.org/10.5194/amt-3-1351-2010, 2010.

Wunch, D., Toon, G. C., Sherlock, V., Deutscher, N. M., Liu, C., Feist, D. G., and Wennberg, P. O.: Documentation for the 2014 TCCON Data, Release GGG2014.R0, CaltechDATA, https://doi.org/10.14291/TCCON.GGG2014.DOCUMENTATION.R0/1221662, 2015.

Wunch, D., Mendonca, J., Colebatch, O., Allen, N., Blavier, J.-F. L., Roche, S., Hedelius, J. K., Neufeld, G., Springett, S., Worthy, D. E. J., Kessler, R., and Strong, K.: TCCON data from East Trout Lake, SK (CA), Release GGG2014R1, CaltechDATA [data set], https://doi.org/10.14291/tccon.ggg2014.easttroutlake01.R1, 2018.

Yu, H., Emde, C., Kylling, A., Veihelmann, B., Mayer, B., Stebel, K., and Van Roozendael, M.: Impact of 3D cloud structures on the atmospheric trace gas products from UV–Vis sounders – Part 2: Impact on NO_2 retrieval and mitigation strategies, Atmos. Meas. Tech., 15, 5743–5768, https://doi.org/10.5194/amt-15-5743-2022, 2022.